Paper originally presented at the 73rd International Astronautical Congress, 18-22 September, Paris – France. www.iafastro.org
Copyright ©2022 by Mr. Hadrien AFSA. Published by the IAF, with permission and released to the IAF to publish in all forms.

IAC-22-C1,IP,10,x67886

Automatic multi-gravity assist trajectory design with modified Tisserand Graphs exploration

Hadrien Afsa[a]*, Andrea Bellome[a], Joan-Pau Sanchez-Cuartielles[b], Stephen Kemble[a]

[a] *Cranfield University, United Kingdom*
[b] *ISAE-Supaero University of Toulouse, France*
* *Corresponding author. E-mail address: hadrien.afsa(at)hotmail.com*

Abstract

Reaching the boundaries of the Solar system has been made possible by Multi-Gravity Assist (MGA) trajectories that reduce the propellant costs by using the gravity of planets to increase or decrease the energy of a spacecraft's orbit. Designing an optimal MGA trajectory constitutes a mixed-integer non-linear programming (MINLP) problem, which requires a simultaneous combinatorial search of discrete elements (e.g., planets), as well as an optimisation of continuous variables, such as departing date, transfer times, Deep Space Manoeuvres (DSM), etc., in an exponentially increasing search space. An efficient way to tackle MINLP problems is to first transcribe them into a simplified combinatorial-only problem and, a posteriori, re-optimise the continuous design variables for a subset of promising sequences of discrete elements.

The transcription of an MGA-MINLP problem into a pure combinatorial one can be efficiently explored via Tisserand Graphs (TG), which employ the Tisserand invariant to map possible flybys as a function of the spacecraft's velocity relative to a given planet. Intersections between contour lines of different relative velocity and planet indicate that a gravity assist is feasible energy-wise and depict how the spacecraft orbit will be modified if undergoing that specific gravity assist. Hence, contour line intersections become the nodes of a graph, which can be efficiently explored via tree traversal algorithms.

However, the information obtained from such a Tisserand exploration does not provide launch window or time of flight, and only yields a rough order of magnitude estimate of Δv. To solve this, a database approach using real ephemerides of celestial objects to correlate initial phase angles of planets with dates and Δv approximation methods to simulate DSMs were implemented. This allows to successfully establish a list of feasible planetary sequences while providing estimations of propellant costs, launch windows and excess velocities.

The solutions identified are validated by re-optimising the complete MGA trajectories as sequences of flybys, DSMs and Lambert arcs intersecting the real positions of the planets involved. Mission scenarios to Jupiter and never-explored objects, e.g. Centaurs or low-perihelion asteroids, are used to validate the accuracy of the Tisserand-based first-guess solutions, as well as the capability to find the global optimum solution in limited computational effort.

Keywords: Tisserand Graphs, multi-gravity assist, mission analysis, trajectory design, tree search algorithms.

Nomenclature

a	Spacecraft's semi-major axis
a_P	Planet's semi-major axis
α	Flyby pump angle
δ	Flyby deflection angle
δ_{max}	Maximum flyby deflection angle
e	Spacecraft's orbit eccentricity
h_{min}	Minimum flyby altitude
i	Spacecraft's orbit inclination
μ_P	Planet's gravitational parameter
n_i	Planet's rate
R	Planet's radius
r_a	Spacecraft's apoapsis
r_p	Spacecraft's periapsis
T	Tisserand criterion
$T_{S/C}$	Spacecraft's orbit period
T_P	Planet's orbit period
T_S	Synodic period
Δv	Change in velocity after a flyby or DSM
v_P	Planet's velocity in heliocentric frame
v_∞^+	Spacecraft's excess velocity after flyby
v_∞^-	Spacecraft's excess velocity before flyby
v_∞	Spacecraft's excess velocity norm
v_1	Spacecraft's velocity before a flyby in heliocentric frame
v_2	Spacecraft's velocity after a flyby in heliocentric frame

Acronyms/Abbreviations

AU	Astronomical Unit
CR3BP	Circular Restricted 3-Body Problem
DSM	Deep Space Manoeuvre
GTOC	Global Trajectory Optimisation Competition
I	Inbound
MGA	Multi-Gravity Assist
MINLP	Multi-Integer Non-Linear Programming
O	Outbound
TG	Tisserand Graph

© 2022 The Authors. This is an Open Access article distributed under the terms of the Creative Commons Attribution Licence (CC BY 4.0), which permits copying, adaptation and redistribution, provided the original work is properly cited (http://creativecommons.org/licenses/by/4.0/).

Paper originally presented at the 73rd International Astronautical Congress, 18-22 September, Paris – France. www.iafastro.org
Copyright ©2022 by Mr. Hadrien AFSA. Published by the IAF, with permission and released to the IAF to publish in all forms.

1. Introduction

The ever-growing ambition to further explore the Solar system and the limitation of current space propulsion technologies led scientists to design several techniques to reach otherwise inaccessible places. One of the major advancements in the design of interplanetary trajectories lies in the utilisation of planets' gravity to change a spacecraft's orbit without using propellant. Such manoeuvre, called gravity assist or flyby, can be repeated with several planets in a so-called Multi-Gravity Assist (MGA) trajectory to extend the accessibility of outer planets. Combined with Deep Space Manoeuvres (DSM), gravity assists proved to be necessary to explore the farthest planets of the system. As a matter of fact, missions like Cassini, Galileo or Rosetta would not have been possible without the benefit of MGA trajectories [1]–[3]. MGA trajectories have been used in all the missions to Jupiter and beyond since Mariner 10 [4], and will also be in future missions such as JUICE [5] (see Figure 1) or Europa Clipper [6].

However, designing an MGA interplanetary trajectory often proved to be a hurdle, as it requires to optimise a problem with a combination of discrete parameters (e.g., planets) as well as continuous variables, such as departing dates, velocities and transfer times. It therefore constitutes a mixed-integer non-linear programming (MINLP) problem. An efficient way to tackle such problems is to first transcribe them into a simplified, pre-analysis combinatorial problem, and then to optimise it with continuous variables. For this purpose, the Tisserand Graph (TG) proves to be particularly efficient.

2. The Tisserand graph

The TG, first introduced in 1998 by Labunksy et al. [7] and further developed by Strange and Longuski [8] in the early 2000s is a visual tool to establish a preliminary design of MGA trajectories. It is based on the Tisserand criterion (1) introduced by François Félix Tisserand [9], an energy-based function that remains approximately constant before and after a flyby and binds the spacecraft's orbit parameters (a, e, i) with the semimajor axis of the body ($a_P, 0, 0$). The inclination of the orbit is generally assumed to be zero ($i = 0°$ in (1)). Otherwise contours on the TG become surfaces (see for example [10] or [11]), which drastically reduces the intuitiveness and simplicity of the method.

$$T = \frac{a_P}{a} + 2\sqrt{\frac{a}{a_P}(1-e^2)}\cos i \qquad (1)$$

TGs are generally $r_p - r_a$ graphs, with r_p the periapsis and r_a the apoapsis (although any combination of orbit parameters can be used) on which orbits can be represented as dots. Specific orbits can allow a spacecraft to meet a planet with a given velocity at the boundary of the planet's sphere of influence, in the planetocentric frame (i.e. as seen from the planet). This velocity is called excess velocity or infinity velocity and denoted by v_∞. These orbits can be grouped together on the TG to form v_∞ contours. Figure 2 shows a TG plotted for Venus, Earth, Mars and Jupiter and with infinity velocities set to 3, 5 and 7 km/s. Intersections between these contours represent orbits that meet the two planets with respective v_∞.

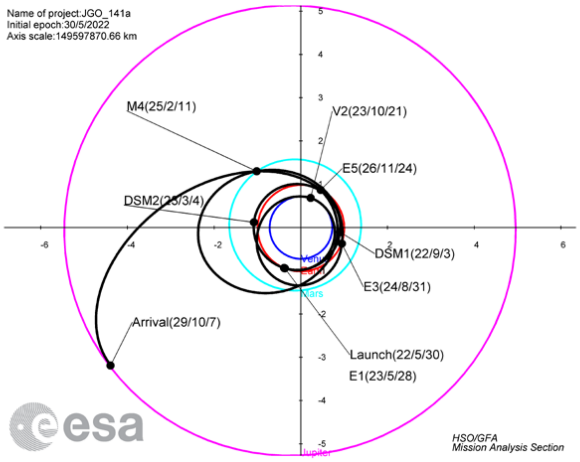

Figure 1 – Example of MGA trajectory: JUICE's journey to Jupiter (from [5])

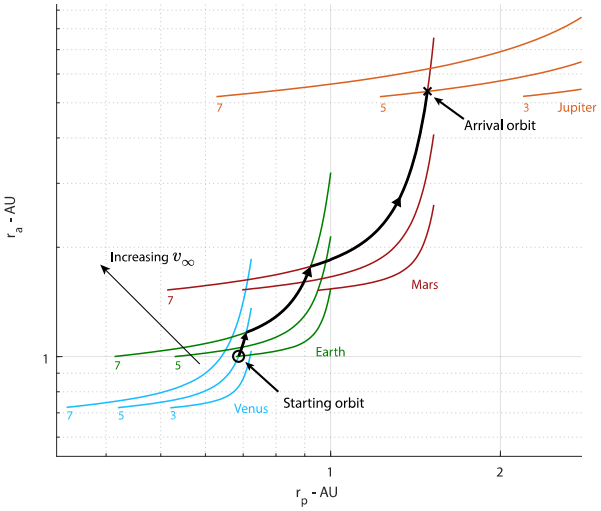

Figure 2 – The Tisserand graph of a EVEMJ sequence. The numbers are the v_∞ in km/s. The limitations of the flyby are not considered here.

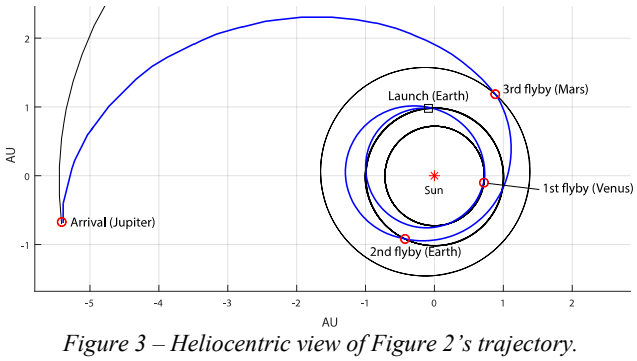

Figure 3 – Heliocentric view of Figure 2's trajectory.

Copyright ©2022 by Mr. Hadrien AFSA. Published by the IAF, with permission and released to the IAF to publish in all forms.

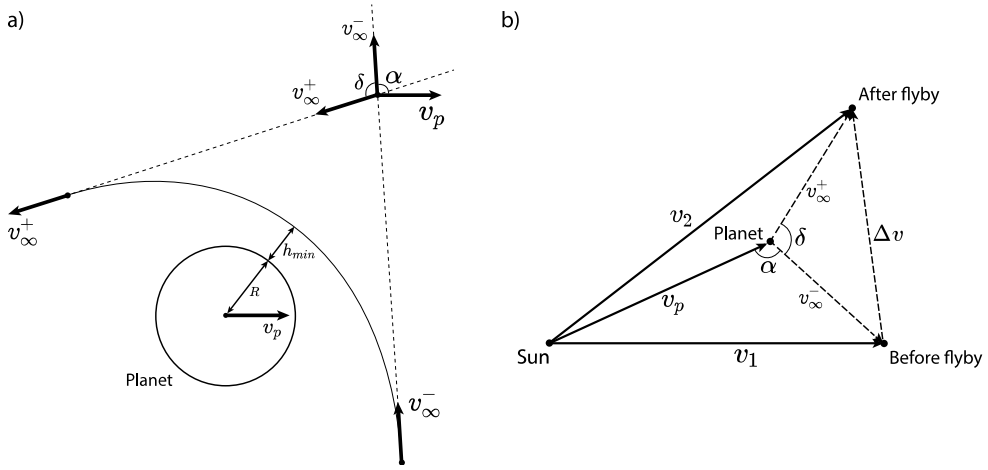

Figure 4 – a) Geometry of a flyby in the planet reference, b) Schematics of the velocities of a flyby

Each v_∞ contour is also related to the pump angle α, the angle between the arrival relative velocity v_∞^- of the spacecraft prior to the flyby and that of the planet v_P (Figure 4). When $\alpha = 0°$, the spacecraft velocity is in the same direction – it corresponds to the highest apoapsis orbit. When $\alpha = 180°$, the spacecraft goes in the opposite direction – it corresponds to the lowest periapsis. During a flyby, the pump angle α is changed by a deflection angle δ from v_∞^- to v_∞^+ (Figure 4). It can be represented as a shift on the planet's contour (Figure 5) – the orbit changes but stays on the v_∞ contour.

The maximum deflection angle δ_{max} is limited by the minimum altitude h_{min} the spacecraft can safely fly over the planet and depends on the flyby body's gravitational parameter as well as the v_∞ of the spacecraft (2). These flybys limitations can be visualised on a TG by tick marks (Figure 5).

$$sin\left(\frac{\delta_{max}}{2}\right) = \left(1 + \frac{(R + h_{min})v_\infty^2}{\mu_P}\right)^{-1} \quad (2)$$

with R and μ_P being the planet's radius and gravitational parameter, respectively.

Flybys can be repeated with nearby intersections to create a sequence. TG can therefore be used to map possible trajectories with theoretically no or very few Δv costs (Figure 2). It is worth noting that impulsive manoeuvres and Hohmann transfers would be represented as vertical and horizontal shifts. An apoapsis-raising manoeuvre is represented in Figure 5.

However, while MGA trajectories obtained from TG are feasible energy-wise, the phasing, i.e. the rendezvous between the spacecraft and the different flyby planets, is not guaranteed. The TG also provides very little information about time of flight or launch window and does not take account of DSMs.

Despite these limitations, the TG remains a powerful tool and has been used, improved, and extended in other works to design interplanetary trajectories, moon tours and orbit insertions with low propellants requirements:

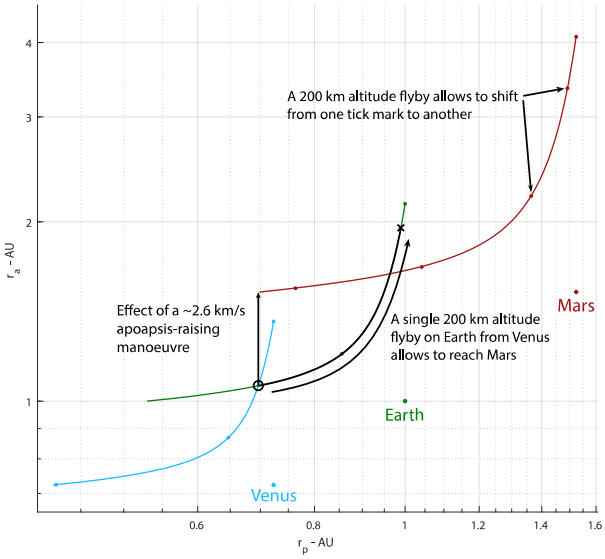

Figure 5 – Principle of a flyby on a TG. Contours plotted are for $v_\infty = 5\ km/s$

The TG can be used for exploration of the Solar system but also for satellite tours, the major body being then a planet. Campagnola et al. have used the TG and combined it with v_∞–leveraging manoeuvres to design Jovian and Saturnian moon tours. Using DSMs between each flyby opens more possibilities in the design of MGA trajectories and allowed to reduce orbit insertion costs and time of flight [12], [13]. Heaton et al. showcased the benefits of using TGs to make quick tour designs and applied their method for the cancelled Europa Orbiter probe, minimising the Δv cost required for orbit insertion. Their study highlights a high-performance tour that allows a Europa arrival with a v_∞ inferior to 2 km/s, while reducing the radiation risks during the flybys [14]. A visualisation of radiations levels on a TG was implemented by Kloster et al. to design a performant Jovian tour using the highly radiative but flyby-efficient moon Io. The method developed allows to measure the radiation accumulated during the trip [15]. The contest-

Copyright ©2022 by Mr. Hadrien AFSA. Published by the IAF, with permission and released to the IAF to publish in all forms.

winning trajectory for the 6th Global Trajectory Optimization Competition (GTOC) was designed using the TG for a Galilean moons mapping [16]. A mission to orbit several Jovian moons was also developed by Ross et al. [17]. Other planets tours were also studied. Strange et al. used the TG for a Saturn tour to Enceladus [18] while Heaton and Longuski proved the feasibility of similar tours in the Uranus system [19]. Finally, trajectories to Neptune were designed by Hughes et al. using the TG to prune unfeasible paths [20].

Maiwald extended the usability of the TG with continuous, non-elliptical orbits to allow the design of MGA trajectories with low-thrust propulsion [21], [22]. Missions to asteroids and closer planets are also studied. Strange et al. used the TG together with the Tisserand criterion to identify asteroids that could be redirected to a Moon orbit with a low Δv using Moon flybys [23], and Bellome et al. used it in an automatic asteroid rendezvous and return mission design tool [24]. Missions to main-belt and near-Earth asteroids using MGA trajectories are designed using the TG by Chen et al. [25] and Sun et al. [26]. Mars missions are studied with the TG by Okutsu and Longuski to identify a free return trajectory using Venus gravity-assist [27].

Tisserand-Poincaré graphs were introduced by Campagnola et al. as an extension of the TG to the Circular Restricted 3-Body problem (CR3BP). They also extend the limitations of the patched-conic method used in the TG to allow ballistic transfers between moons. They were used to further decrease the cost of orbit insertions during Jovian tours [10]. The Tisserand-Poincaré graph was then extended by Yárnoz et al. [28] and studied by Pugliatti [29] to take account of the Sun perturbation and use it to design consecutive Moon gravity assist trajectories to exit Earth's attraction with very low Δv. This technique is used in missions such as DESTINY [30] and EQUULEUS [31].

Another approach to extend the patch-conic method of TGs to low-energy orbits lies in the Flyby map introduced by Campagnola et al. [32] and inspired by the Keplerian map for the CR3BP [33]. A Jovian tour was designed with this tool to further decrease the required cost of a Europa orbit insertion [34].

The three-dimensional version of the TG mentioned previously that takes account of the inclination of orbits is used by Campagnola and Kawakatsu for the design of a tour ending with a high inclination final orbit for the cancelled Jupiter Magnetospheric Orbiter mission [11], [35].

These modified versions of the TG add complexity to the problem for specific purposes and are used by experienced users for manual tuning of trajectories. Another approach is considered by other authors to solve the combinatorial part of the MINLP problem and to automatise the preliminary analysis of interplanetary trajectories. De La Torre et al. [36] use the unmodified TG with tree search algorithms to build a list of energy-feasible transfers between two planets, while Bellome et al. [37] un-discretised the TG for accurate, preliminary design of trajectories that are later optimised with DSMs and Lambert arc transfers. The presented work lies between these two and aims to improve the quantity and quality of the critical information that can be obtained from automatic analysis by exploring new implementations of the TG. As the preliminary analysis is solely made, the two-body, circular and restricted model is used for simplicity and reduced computational effort.

3. Generating feasible MGA trajectories

As it was done in [36], the automation of the combinatorial search of trajectories is made by generating a list of all the intersections displayed on a TG. Each intersection is a unique combination of two planets, v_∞ contours, and pump angle α. The corresponding orbits elements can be obtained with (3) and (4) (see demonstration in the appendix):

$$a = a_P \left(1 - \left(\frac{v_\infty}{v_P}\right)^2 - 2\frac{v_\infty}{v_P}\cos(\alpha)\right)^{-1} \quad (3)$$

$$e = \sqrt{1 - \frac{a_P}{a}\left(\frac{1}{2}\left(3 - \frac{a_P}{a} - \left(\frac{v_\infty}{v_P}\right)^2\right)\right)^2} \quad (4)$$

with a_P being the semi-major axis of the flyby planet.

The search starts from a planet with a specified list of departing v_∞ (e.g. Earth with velocities between 3 km/s and 6 km/s for current launchers performances). A combinatorial search using Depth-Limited Tree search algorithm is then used to establish an exhaustive list of

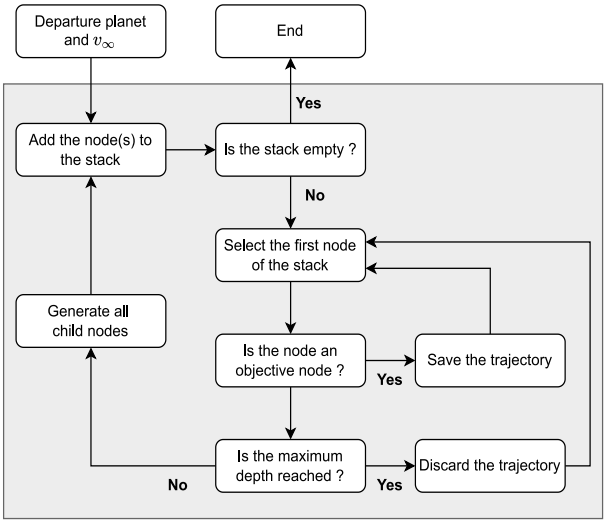

Figure 6 – Flowchart of the combinatorial search. A node constitutes a unique planet and v_∞ value. The stack is a list of nodes that are yet to be explored.

Copyright ©2022 by Mr. Hadrien AFSA. Published by the IAF, with permission and released to the IAF to publish in all forms.

possible trajectories to the desired goal (a planet with an acceptable range of v_∞). The use of heuristic algorithms that prune results based on performance variables (time of flight or Δv costs) is avoided as the inaccuracies of the information obtained from the circular and coplanar model could discard promising trajectories.

In order to prevent endless loops from happening during the tree search, repetition of flybys with the same planet and same v_∞ contour must be separated by two other flybys. Moreover, the maximum depth of the tree, and therefore the number of flybys, is limited during the search. All results exceeding this limit are not considered. A flowchart of the implemented algorithm is given in Figure 6.

Naturally, the precision achieved by a Tisserand graph exploration, besides being limited by the simplified model used, is largely related to the number of v_∞ contours taken in account in the computation. For contours going from 3 km/s up to 15 km/s, with a step of 0.5 km/s, thousands of intersections are obtained, generating millions of feasible trajectories. The maximum number of flybys authorised in a trajectory also increases the number of solutions, but it is sought to be as low as possible to limit the total time of flight. The computational effort, and therefore the processing time grows exponentially. Careful consideration must be taken when selecting the analysis parameters. It is worth noting that high v_∞ contours generate significantly more intersection. Figure 7 gives an estimation of the number of intersections and unfiltered trajectories (unfiltered trajectory does not take account of the flyby limitations or DSMs). For sufficiently high numbers of v_∞ levels, the number of unfiltered solutions reaches hundreds of millions, which is consequent but still manageable for a performant computer. It is moreover unnecessary to further decrease the coarseness of the v_∞ grid, as the main sources of errors still lies in the simplified model used. The number of intersections – and therefore of solutions, can remain relatively low and easy to handle. Consequently, complete tree searches can be performed, removing the need of heuristic or meta-heuristic algorithms such as Genetic Algorithms, Ant Colony or Particle Swarm Optimisation. The method is exhaustive, meaning that the global optimum cannot be pruned, while still relatively fast.

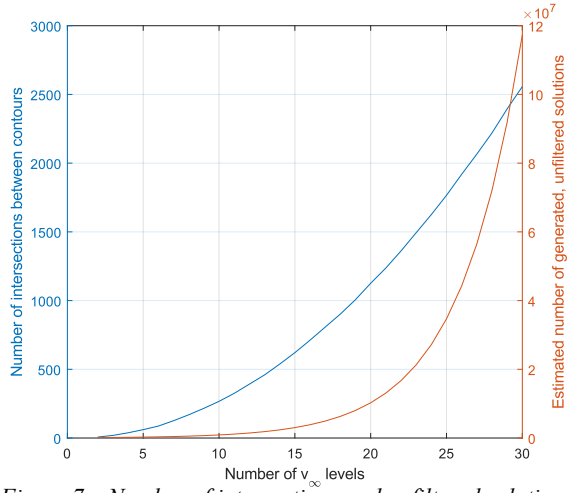

Figure 7 – Number of intersections and unfiltered solutions generated as a function of the number of v_∞ levels between 3 and 15 km/s. The planets considered are Venus, Earth, Mars and Jupiter, with a departure from Earth lower than 6 km/s.

4. Resonances and Deep Space Manoeuvres

As expressed earlier, the shift on a v_∞ contour during a flyby is limited by the minimum altitude of the flyby. This minimum altitude is linked to the properties of planets, such as their atmosphere boundary altitude, the radius of their ring or the distance required to limit the radiations received. Table 1 gives the minimum altitude considered for each planet to compute the maximum deflection angle for a flyby. Because of this constraint, not all the trajectories from one orbit to another are directly possible on a TG. To assess this limitation, resonances and DSMs are considered.

Table 1 – Minimum flyby altitude for each planet. The limits taken for the gaseous planets are set to avoid their high radiation levels or rings.

Planet	$h_{min}(km)$
Mercury	200
Venus	200
Earth	200
Mars	200
Jupiter	$5R_J = 349555$
Saturn	$2R_S = 116464$
Uranus	$R_U = 25362$
Neptune	$R_N = 24624$

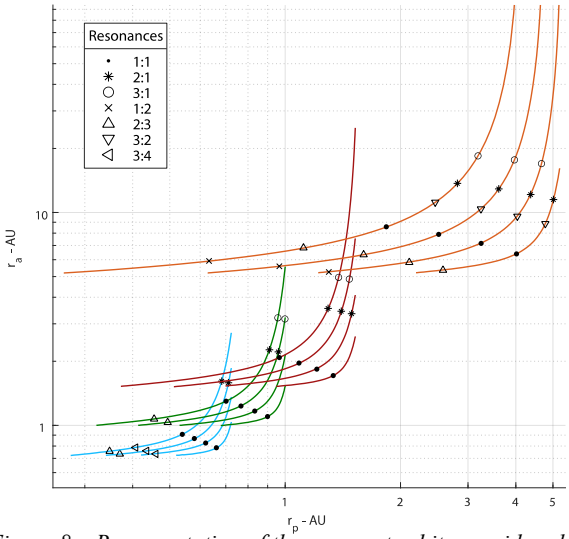

Figure 8 – Representation of the resonant orbits considered for Venus, Earth, Mars and Jupiter. v_∞ levels are 3, 5, 7 and 9 km/s.

Copyright ©2022 by Mr. Hadrien AFSA. Published by the IAF, with permission and released to the IAF to publish in all forms.

A resonance, or resonant orbit, is a particular orbit of the spacecraft for which its period is equal to an integer ratio to that of the planet. After n revolutions of the planet and m revolutions of the spacecraft, the two will meet again and another flyby will be possible. For instance, a 3:1 resonance would correspond to a high apoapsis orbit of the spacecraft where $T_{S/C} = 3T_P$. In practice, only specific (n, m) combinations are used, and high values are avoided as they would drastically increase the total time of flight. Commonly used resonances in past missions and papers were used for each planet [38]–[43]. Resonances can be represented on a TG by tick marks on each contour. Figure 8 displays the resonances used.

When a single flyby is insufficient to reach the next intersection on the TG, the use of a resonant orbit for a second consecutive flyby with the same planet is analysed. The process can be repeated several times if other resonant orbits are met. Figure 9 illustrates this principle.

However, resonant orbits are not systematically reached after a flyby, or the next intersection on the TG may not be attained even after a resonant flyby. Low Δv DSMs are then considered to correct for the slight difference of energy, and near-missed intersections or resonant orbits can therefore be reached. The Δv cost is computed using Hohmann transfers. This implementation also limits the pruning of promising trajectories because of minor numerical differences.

An estimation of the time of flight of each leg of the trajectory can be made using Kepler's equation. With no prior information on where the flybys are performed on the spacecraft orbit, all types of transfers must be considered. Each planet departure or arrival can be Outbound (O), i.e. after the periapsis and before the apoapsis, or Inbound (I), i.e. after the apoapsis and before the periapsis, leading to four different combinations. Table 2 gives the flight time formulas for both upward and downward transfers. The time of flight for resonances is computed using the period of the spacecraft on its resonant orbit.

The precision of such computation is limited by the circular and coplanar planetary ephemerides considered

Table 2 – Time of flight of the different types of transfer.

Up transfer	Down transfer	Time of Flight
O – O	I – I	$t_2 - t_1$
O – I	O – I	$T_{S/C} - t_2 - t_1$
I – O	I – O	$t_1 + t_2$
I – I	O – O	$T_{S/C} - t_2 + t_1$

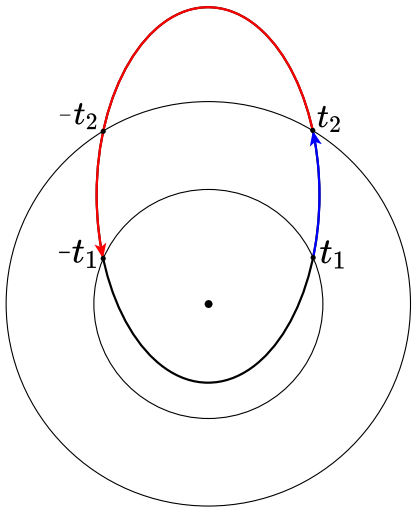

Figure 10 – Inbound and outbound transfers. The blue trajectory is an O – O up transfer, the red trajectory is an O – I down transfer.

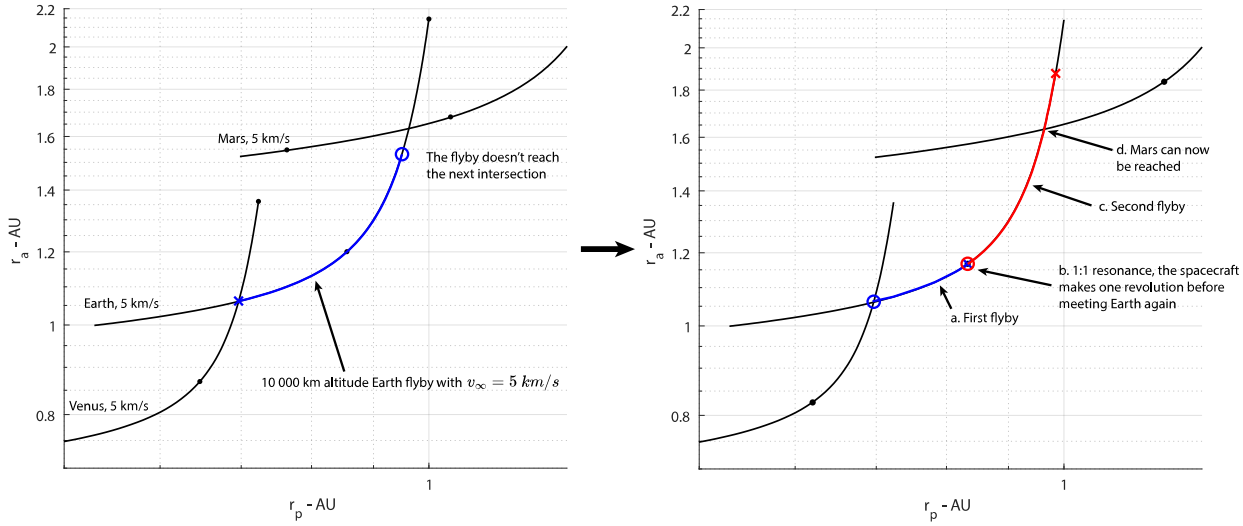

Figure 9 – Principle of resonant orbit flyby. Assuming a minimum flyby altitude of 10 000 km (for this example), a single flyby is not sufficient to reach the next intersection. The 1:1 resonance is used. The time of flight is lengthened by a year.

Copyright ©2022 by Mr. Hadrien AFSA. Published by the IAF, with permission and released to the IAF to publish in all forms.

in the TGs. For this reason, the slight change of time of flight due to DSMs is not taken into account, as insignificant compared to the errors made.

5. Estimation of a launch window

The launch window is one of the most critical information provided by a mission analysis as it drives its process of development. Having a good estimation of a launch window can drastically reduce the search space and help to converge to an optimised trajectory. As the TG provides no information about dates, a comparison method with real ephemerides and phase angle difference between the departing planet and the first flyby planet is implemented.

From the orbits of the launch planet and first flyby planet, the spacecraft's orbit parameters and the time of flight of the first leg obtained from the TG, it is possible to compute the phase angle between the two planets at the time of the launch. As a given phase angle only repeats once every synodic period, it is possible to correlate this phase angle with a date. In practice, when Mercury is not involved in the computation, synodic periods are generally longer than a year (Figure 11). The equation to compute the synodic period T_S between two planets is given in (5).

$$T_S = \frac{2\pi}{|n_1 - n_2|} \tag{5}$$

Using the real ephemerides of the planets and starting from a reference date, a database of all phase angles and their related date is generated. This database will span from the reference date to a full synodic period between the two planets.

Four different launch dates can be associated with the first leg of the trajectory – one for each I – O transfer type. They are all computed and considered in the results. The errors that occur in the computation of the phase angle because of the circular and coplanar model can be taken into account by a correction margin on the obtained dates.

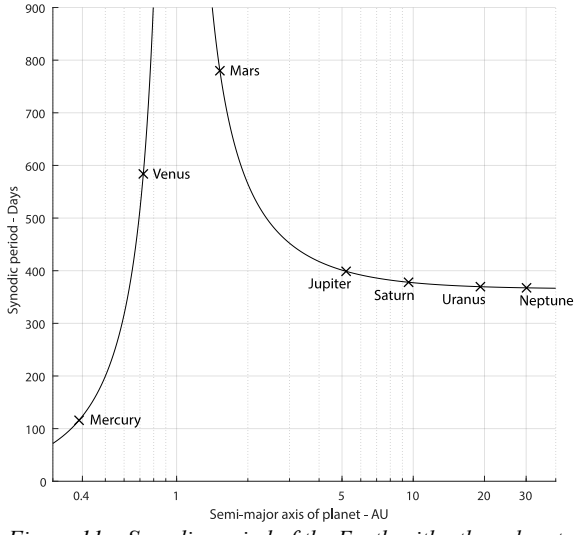

Figure 11 – Synodic period of the Earth with other planets

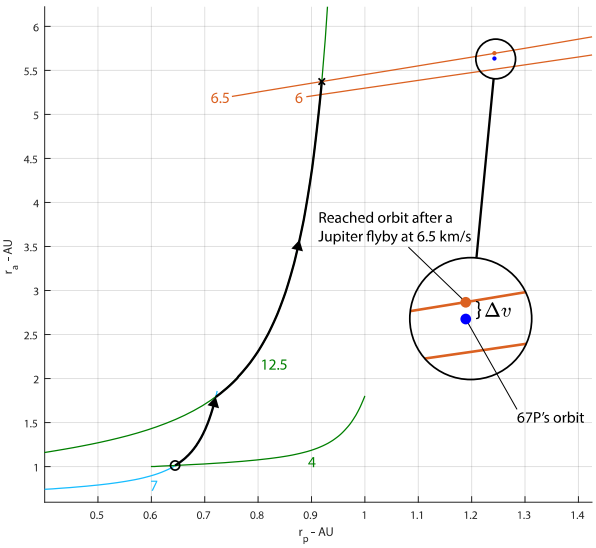

Figure 12 – Example of trajectory to 67P/Tchourioumov-Guerassimenko. After an EVEJ trajectory, the orbit reached on the Jupiter 6.5 km/s contour allows to reach the objective with a small DSM.

As it will be seen later, the launch windows obtained with this method are relatively broad but still consequently limits the possibilities and drastically reduce the search space.

6. Asteroid and comet rendezvous

Asteroid investigations or sample return missions are also of main interest for scientists and a significant challenge for trajectory designers. In this purpose, the TG can also provide useful information to help with the optimisation process of a candidate trajectory.

Like planets, the orbit of an asteroid can be represented as a dot on a TG. MGA rendezvous missions to such objects can therefore be designed – the objective is then no longer a v_∞ contour but a specific orbit. As the coarseness of the v_∞ levels prevents the search to numerically reach this point, a possible approach is to find the nearest v_∞ contours on the TG and find the orbits on these contours that would minimise the Δv cost for a correction manoeuvre. The Δv costs are computed using Hohmann transfers. Once a specific contour is selected, it is set as an objective for the preliminary trajectory design. It is then necessary to check that the last flyby allows to reach the closest orbit, or that the use of a resonance is possible otherwise.

Note that this method privileges Δv cost instead of time of flight. When the closest orbit on the objective v_∞ contour cannot be reached after the last flyby, a high Δv manoeuvre would be necessary to join the final orbit without overextending the transfer time. Using higher v_∞ contours allows to reach a nearer orbit, reducing the costs of the final DSM. This case is detailed in Section 7.2.

Copyright ©2022 by Mr. Hadrien AFSA. Published by the IAF, with permission and released to the IAF to publish in all forms.

7. Results

The developed algorithm is tested on specific study cases in this section. In order to properly compare with relevant information, the values obtained are faced to that of actual missions. The trajectory of the upcoming mission to Jupiter JUICE is used for its complexity.

As the data provided in literature for such missions is very limited, the trajectory is also analysed with a third-party optimisation software described in [44]. This software uses the real ephemerides of the planets and combinations of Lambert arcs in the patched-conic approximation to compute accurate trajectories to any object. The differences between the arrival and departure excess velocities v_∞ during flybys of the Lambert arcs are compensated with DSMs performed impulsively immediately after the flyby if the deflection provided by the gravity assist is not enough. The refined trajectories obtained from this software are very accurate and allow to verify the pertinence of the information provided by the TG.

To demonstrate the versatility of the software, test cases to smaller objects are also studied. Missions to the 67P comet as well as a low perihelion asteroid are described.

7.1. JUICE test case

A first case study of a trajectory to Jupiter is made. The obtained trajectory can be compared to the upcoming JUICE first designed trajectory [5]. This trajectory has been adapted due to the postponement of the launch, removing the Mars flyby [45]. For benchmark purposes, the 2022 launch trajectory is used in this comparison. This trajectory is:

Earth – Earth – Venus – Earth – Mars – Earth – Jupiter

and will be denoted EEVEMEJ hereinafter.

The first Earth flyby is mainly used for declination correction. On a TG where inclination is not considered and if no DSM is performed, this manoeuvre shifts the orbit on the departing v_∞ contour, which would not be different to a launch with a different angle. For these reasons, this first flyby is ignored for the comparison and the sequence considered henceforth is EVEMEJ. The launch date of JUICE considered in the following corresponds to the date of the first Earth flyby.

The search algorithm is launched with the parameters given in Table 3. They are corresponding to the current performances of launchers and the requirements in terms of arrival speed at the objective target. The v_∞ levels grid with a 0.5 km/s step allows a fast computation without a major accuracy loss. The cost of a single DSM is limited to privilege low-cost trajectories. The total capacity roughly corresponds to that of JUICE.

The number of unique sequences obtained, as well as the number of total feasible trajectories with or without DSMs are given in Table 4. These results were obtained in roughly one hour on a standard laptop. Each sequence – i.e. unique combination of planets, regardless of the flyby velocities, regroups several trajectories – i.e. for a given sequence, several combinations of excess velocities at each flyby are possible.

The JUICE sequence is found several times in the results. The obtained range of time of flight and v_∞ are compared to the real times of flight of the mission (Table 5) and the excess velocities computed with an optimisation software (Table 6).

No DSM was calculated for this trajectory as all the flybys performed respected the minimum altitude constraint. The estimated Δv with the optimisation software is approximately 110 m/s.

A deeper analysis of the results yields the closest trajectory regarding excess velocities (Table 6), i.e. the trajectory for which the infinity velocity computed for each flyby is the closest to that computed by the optimisation software. All the velocities obtained are as close as the v_∞ grid allows, except for the Jupiter arrival velocity, for which 5.5 km/s would be a better fit. This slight error is due to the fact that no intersection between Earth 11.5 and Jupiter 5.5 exists on the TG with its low-fidelity model. Given the transfer types for each leg, the computed and real times of flight can be compared (Table 5). Again, the results are relatively close – within a 10% error margin, except for the Venus – Earth and the Mars – Earth legs. These larger errors are mainly due to the

Table 3 – Search parameters of the software used for the JUICE scenario test case

Planets considered	Venus, Earth, Mars, Jupiter
Minimum infinity velocity	3 km/s
Maximum infinity velocity	15 km/s
Interval step of infinity velocity	0.5 km/s
Departure	Earth, 3 to 6 km/s
Arrival condition	Jupiter, 3 to 7 km/s
Maximum number of non-resonant flybys	4
Maximum single DSM cost	0.5 km/s
Max. total DSMs cost	3 km/s

Table 4 – Number of found solutions for the JUICE scenario test case

	Without DSM	With DSMs
Number of sequences found	146	162
Total number of trajectories	2 185 147	2 791 170
Number of JUICE-like (EVEMEJ) trajectories	120 103	243 939

Copyright ©2022 by Mr. Hadrien AFSA. Published by the IAF, with permission and released to the IAF to publish in all forms.

difference between the real ephemerides of the planets and the coplanar and circular model. Mars has a slightly high eccentricity (0.09) while Venus' orbit has a 3.4° angle with the ecliptic plane.

The estimated launch window for this specific trajectory is between 05/05/2023 (Day/Month/Year) for an O – I transfer and 05/07/2023 for an I – O transfer. The two other transfer types lie between these dates. The first Earth flyby of the actual JUICE trajectory is 03/06/2023, which is within the obtained range and 29 days after the estimated launch date for an O – I transfer. The error made is therefore relatively important (~1 month), but still close to the optimal solution. The launch window estimation can therefore significantly reduce the search space.

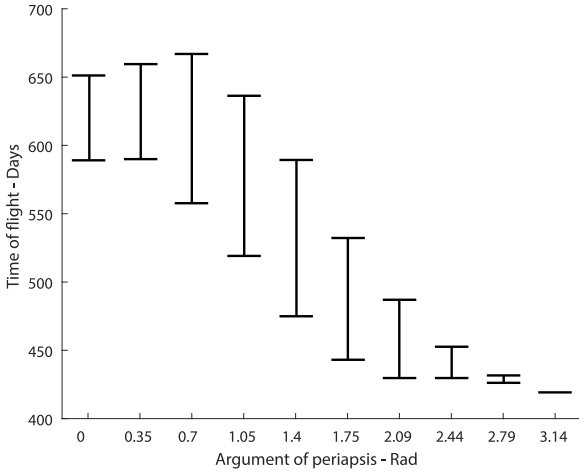

Figure 13 – Ranges of computed time of flight for a trajectory from Earth to Mars with fixed departure and arrival velocities. The argument of periapsis of the Mars orbit is varied. This example shows the influence that the eccentricity of the orbit can have on the results.

While the software developed shows its ability to make relatively accurate first guesses of complex MGA trajectories with detailed information, the limits of the circular and coplanar model used in the TG are highlighted in these results. It has been demonstrated that the differences observed in the results are mainly due to the planets' eccentricities (especially for Mars) and inclination (especially for Venus) in the real ephemerides. For instance, Figure 13 shows the evolution of the computed ranges of time of flight for an Earth – Mars transfer when considering Mars eccentricity by varying the argument of periapsis of its orbit. For this reason, it is necessary to optimise and further study the trajectory to remove these errors and to consider the phasing of the planets using the real ephemerides. The information obtained from the TG can be used to accelerate this process.

7.2. Asteroids rendezvous

Missions to smaller and hard-to-reach objects can also be studied with this technique. A first study case of a trajectory to 67P/Tchourioumov-Guerassimenko, famous for being Rosetta's target, is described in the following. Several sequences were studied in [24], and a promising sequence was identified as being an EVEM trajectory to join 67P after the last Mars flyby. A refined version of this trajectory is obtained with the optimisation software for comparison. As stated in Section 6., finding the closest v_∞ might not yield the optimal trajectory if time of flight is considered. A preliminary search is therefore made to Mars contours close to 67P's orbit. The results are given in Table 7. A similar trajectory is found once again, and the v_∞ bounds provided are coherent. The DSM cost for the manoeuvre to 67P (after the Mars flyby) is very close to the optimised value. The DSM to reach Mars is however very different, mainly due to the

Table 5 – Comparison of the times of flight computed with the actual JUICE trajectory. Transfer times are in days.

Leg	E – V	V – E	E – M	M – E	E – J	Total (years)
Transfer types of the JUICE trajectory	O – I	I – I	I – O	O – O	O – I	/
Ranges computed	61 – 240	50 – 606	60 – 850	59 – 850	723 – 1458	2.6 – 11
JUICE trajectory	145	315	161	654	1065	6.4
Closest trajectory obtained	155	281	167	508	1083	6.0

Table 6 – Comparison of the infinity velocities obtained with the actual JUICE trajectory. Excess velocities are in km/s.

	Earth	Venus	Earth	Mars	Earth	Jupiter
v_∞ ranges computed	3 – 6	3.5 – 12.5	4.5 – 14.5	7.5 – 15	9 – 15	6 – 7
JUICE trajectory	3.3	5.8	8.8	10.1	11.5	5.6
Closest trajectory obtained	3.5	6	9	10	11.5	6

Copyright ©2022 by Mr. Hadrien AFSA. Published by the IAF, with permission and released to the IAF to publish in all forms.

Table 7 – Comparison of the infinity velocities obtained with the optimal trajectory to 67P. Values are in km/s.

	Earth	Venus	Earth	Mars
Optimised trajectory v_∞	3.2	5.2	9.5	14.1
Optimised trajectory DSM's Δv after flyby	0	~0	0.925	1.210
v_∞ ranges computed	3 – 6	4.5 – 12.5	7.5 – 14.5	12 – 17
Closest trajectory's v_∞ obtained	3.5	5.5	9.5	14
Estimated DSM's Δv after flyby	0	0	0.313	1.181

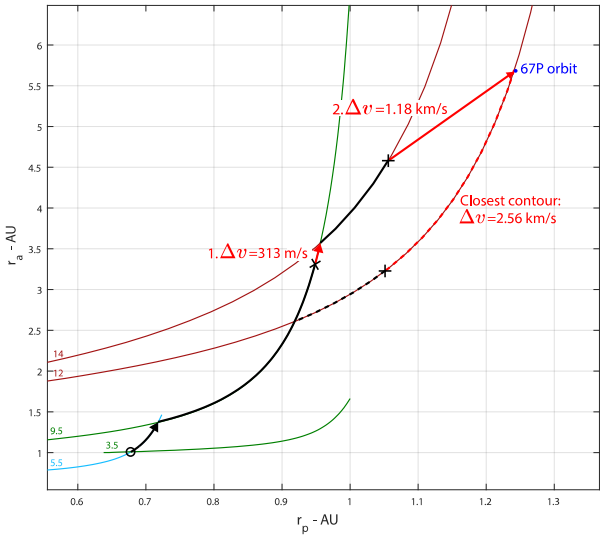

Figure 14 – The EVEM trajectory to 67P with its two DSMs.

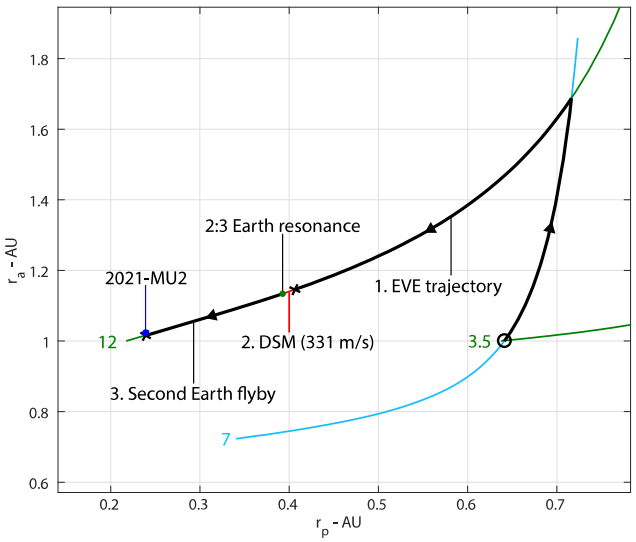

Figure 15 – TG of the trajectory to 2021-MU2

low-fidelity model used. Note that both computed DSMs are assumed to be impulsive manoeuvres.

The estimated launch window for the year 2039 used in the optimisation software is between 24/04 and 28/06. The optimised launch date is 27/05/2039, which lies well between the estimated dates.

The trajectory is plotted in Figure 14. As expressed earlier, the dotted trajectory shows that using the closest contour does not provide the most cost-efficient solution. Note also that a resonance with Mars could have been used to reduce the final Δv cost, but at the price of a longer time of flight.

The return trip can be designed similarly, as the solutions found are symmetrical – a possible return trip could be MEVE with the same DSMs.

A last study case to a low-perihelion asteroid is discussed to demonstrate the preliminary design of a trajectory to such objects. The asteroid selected is 2021-MU2, classified as a potentially hazardous asteroid by NASA. Its aphelion is 1.023 AU, and its perihelion is 0.239 AU. Like before, its real inclination of 8.556° is neglected.

The method of the nearest contours is used here. Earth contours with v_∞ of 12 and 12.5 km/s are the closest identified to reach 2021-MU2's orbit.

The search is run with a departure from Earth with a velocity inferior to 6 km/s, considering up to 3 flybys on Venus, Earth or Mars (other planets would be irrelevant) and for ranges of v_∞ going from 3 to 17 km/s with a step of 0.5 km/s. A total number of 146 655 potential trajectories were obtained, among 37 different sequences. 82 EVEE trajectories are of particular interest for their low time of flight compared to longer, more complex sequences. A promising trajectory with an Earth departure at 3.5 km/s and a Venus flyby at 7 km/s is identified to reach Mars' 12 km/s contour. A DSM of 331 m/s is required for this trajectory to reach the 2:3 resonance orbit on the Earth contour. 2021-MU2's orbit is directly reached after the second Earth flyby (Figure 15). The launch window identified for 2021 (for instance) is between 10/10 and 03/12.

As showcased in this study case, a first approximation of a potential trajectory can be quickly identified using the TG exploration. This trajectory can serve as a first guess to guide the optimisation process.

8. Discussion

The results presented show both the benefits and limitations of the TG exploration. It has been demonstrated that this method of MGA trajectory design can provide quick estimations of feasible trajectories

Copyright ©2022 by Mr. Hadrien AFSA. Published by the IAF, with permission and released to the IAF to publish in all forms.

with accurate approximations of its critical information (see also [46]). The implementations added allow to estimate the time of flight, the launch date and the Δv cost of specific DSMs.

However, the low-fidelity model of the coplanar and circular orbits of the planets, as well as the non-consideration of the planet's phasing clearly limits the validity of the data obtained. When considering the v_∞ of each flyby of a trajectory, significant errors can emerge, and it is then recommended to use the ranges of data provided by the TG exploration rather than the value itself. In the optimisation software mentioned in this paper, using the v_∞ and time of flight ranges obtained allowed to significantly reduce the computational time and to prune irrelevant trajectories. In all cases, the phasing must be checked and corrected.

The current version of the tool therefore provides satisfying results, but more improvements and optimisations are possible. For instance, multi-revolution trajectories could allow to find more solutions for particularly demanding trajectories, and DSM could be implemented to allow transfers to different v_∞ contours for better representation of actual manoeuvres.

9. Conclusion

The work presented extends the usability of the TG for fast, automatic preliminary design of MGA trajectories. The results are compared with real trajectories that are analysed with a third-party optimisation software. Despite the limitation of the simplified model used and the non-consideration of the planets' phasing, the implementations added allow to obtain more critical information that can be used to reduce the search space for further optimisation and refinements. Besides feasible sequences, accurate approximation of excess velocities, time of flight and launch windows are provided. This tool yields first guesses of promising sequences to most objects in the Solar system and can help to drastically reduce the effort required to design optimised trajectories.

The tool uses MatLab and can be found at https://github.com/hadrienafsa/AUTOMATE.

Appendix

From $v_P = \sqrt{\frac{\mu_{Sun}}{a_P}}$ and $v_1 = \sqrt{\mu_{Sun}\left(\frac{2}{a_P} - \frac{1}{a}\right)}$ when the spacecraft encounters the planet, one has:

$$\frac{v_1^2}{v_P^2} = \frac{\mu_{Sun}\left(\frac{2}{a_P} - \frac{1}{a}\right)}{\frac{\mu_{Sun}}{a_P}} = 2 - \frac{a_P}{a}$$

and thus:

$$a = \frac{a_P}{2 - \frac{v_1^2}{v_P^2}}$$

From Figure 4 b), the cosine law gives:

$$v_1^2 = v_P^2 + v_\infty^{-2} - 2 v_P\, v_\infty^- cos(\pi - \alpha)$$
$$\Rightarrow \frac{v_1^2}{v_P^2} = 1 + \frac{v_\infty^{-2}}{v_P^2} + 2\frac{v_\infty^-}{v_P}\cos(\alpha)$$

Replacing it in the previous equation yields (3).

The angular momentum of the spacecraft h when it meets the planet approximates to:

$$h = a_P v_1 \cos\gamma$$

with γ the flight path angle (i.e. the angle between v_1 and v_P in Figure 4 b)). Also, one has:

$$h = \sqrt{\mu_{Sun} a(1 - e^2)}$$

and therefore:

$$v_1 \cos\gamma = \sqrt{\mu_{Sun}\frac{a}{a_P^2}(1 - e^2)}$$

The cosine law gives:

$$\frac{v_\infty^{-2}}{v_P^2} = 1 + \frac{v_1^2}{v_P^2} - 2\frac{v_1}{v_P}\cos(\gamma)$$
$$= 3 - \frac{a_P}{a} - 2\sqrt{\frac{a}{a_P}(1 - e^2)}$$

Rearranging this equation yields (4).

Copyright ©2022 by Mr. Hadrien AFSA. Published by the IAF, with permission and released to the IAF to publish in all forms.

References

[1] F. Peralta and S. Flanagan, 'Cassini interplanetary trajectory design', *Control Eng. Pract.*, vol. 3, no. 11, pp. 1603–1610, Nov. 1995, doi: 10.1016/0967-0661(95)00171-P.

[2] L. A. D'Amario, L. E. Bright, and A. A. Wolf, 'Galileo trajectory design', *Space Sci. Rev.*, vol. 60, no. 1–4, May 1992, doi: 10.1007/BF00216849.

[3] A. Accomazzo, P. Ferri, A. Hubault, S. Lodiot, J. L. Pellon-Bailon, and R. Porta, 'Rosetta visits asteroid (21)Lutetia', *Acta Astronaut.*, vol. 72, pp. 178–184, Mar. 2012, doi: 10.1016/j.actaastro.2011.09.006.

[4] A. A. Siddiqi, *Beyond Earth: a chronicle of deep space exploration, 1958-2016*, Second edition. Washington, DC: National Aeronautics and Space Administration, Office of Communications, NASA History Division, 2018.

[5] E. Ecale, F. Torelli, and I. Tanco, 'JUICE interplanetary operations design : drivers and challenges', presented at the 2018 SpaceOps Conference, Marseille, France, May 2018. doi: 10.2514/6.2018-2493.

[6] B. Buffington, 'Trajectory Design Concept for the Proposed Europa Clipper Mission (Invited)', presented at the AIAA/AAS Astrodynamics Specialist Conference, San Diego, CA, Aug. 2014. doi: 10.2514/6.2014-4105.

[7] A. V. Labunsky, O. V. Papkov, and K. G. Sukhanov, *Multiple gravity assist interplanetary trajectories*. Australia: Gordon and Breach Science Publishers, 1998.

[8] N. J. Strange and J. M. Longuski, 'Graphical Method for Gravity-Assist Trajectory Design', *J. Spacecr. Rockets*, vol. 39, no. 1, pp. 9–16, Jan. 2002, doi: 10.2514/2.3800.

[9] F.-F. Tisserand, *Traité de mécanique céleste*, Repr. d. Ausg. Paris 1889-1896. Sceaux: Gabay, 19.

[10] S. Campagnola and R. P. Russell, 'Endgame Problem Part 2: Multibody Technique and the Tisserand-Poincare Graph', *J. Guid. Control Dyn.*, vol. 33, no. 2, pp. 476–486, Mar. 2010, doi: 10.2514/1.44290.

[11] S. Campagnola and Y. Kawakatsu, 'Jupiter Magnetospheric Orbiter: Trajectory Design in the Jovian system', *J. Spacecr. Rockets*, vol. 49, no. 2, pp. 318–324, Mar. 2012, doi: 10.2514/1.A32055.

[12] S. Campagnola, A. Boutonnet, J. Schoenmaekers, D. J. Grebow, A. E. Petropoulos, and R. P. Russell, 'Tisserand-Leveraging Transfers', *J. Guid. Control Dyn.*, vol. 37, no. 4, pp. 1202–1210, Jul. 2014, doi: 10.2514/1.62369.

[13] S. Campagnola, N. J. Strange, and R. P. Russell, 'A fast tour design method using non-tangent v-infinity leveraging transfer', *Celest. Mech. Dyn. Astron.*, vol. 108, no. 2, pp. 165–186, Oct. 2010, doi: 10.1007/s10569-010-9295-1.

[14] A. F. Heaton, N. J. Strange, J. M. Longuski, and E. P. Bonfiglio, 'Automated Design of the Europa Orbiter Tour', *J. Spacecr. Rockets*, vol. 39, no. 1, pp. 17–22, Jan. 2002, doi: 10.2514/2.3801.

[15] K. W. Kloster, A. E. Petropoulos, and J. M. Longuski, 'Europa Orbiter tour design with Io gravity assists', *Acta Astronaut.*, vol. 68, no. 7–8, pp. 931–946, Apr. 2011, doi: 10.1016/j.actaastro.2010.08.041.

[16] G. Colasurdo, A. Zavoli, A. Longo, L. Casalino, and F. Simeoni, 'Tour of Jupiter Galilean moons: Winning solution of GTOC6', *Acta Astronaut.*, vol. 102, pp. 190–199, Sep. 2014, doi: 10.1016/j.actaastro.2014.06.003.

[17] S. Ross, W. Koon, M. Lo, and J. Marsden, 'Design of a Multi-Moon Orbiter', *Adv. Astronaut. Sci.*, vol. 114, Jan. 2003.

[18] N. J. Strange, S. Campagnola, and R. P. Russell, 'Leveraging flybys of low mass moons to enable an Enceladus orbiter', *Adv. Astronaut. Sci.*, vol. 135, no. 3, pp. 2207–2225, 2009.

[19] A. F. Heaton and J. M. Longuski, 'Feasibility of a Galileo-Style Tour of the Uranian Satellites', *J. Spacecr. Rockets*, vol. 40, no. 4, pp. 591–596, Jul. 2003, doi: 10.2514/2.3981.

[20] K. M. Hughes, J. W. Moore, and J. M. Longuski, 'Preliminary analysis of ballistic trajectories to Neptune via gravity assists from Venus, Earth, Mars, Jupiter, Saturn, and Uranus', *Adv. Astronaut. Sci.*, vol. 13–805, 2013, [Online]. Available: https://www.semanticscholar.org/paper/AAS-13-805-PRELIMINARY-ANALYSIS-OF-BALLISTIC-TO-VIA-Hughes-Moore/cb20dc32ae0b5fff11a0329bbc71032af46b7214

[21] V. Maiwald, 'A new method for optimization of low-thrust gravity-assist sequences', *CEAS Space J.*, vol. 9, no. 3, pp. 243–256, Sep. 2017, doi: 10.1007/s12567-017-0147-7.

[22] V. Maiwald, *About combining Tisserand graph gravity-assist sequencing with low-thrust trajectory optimization*. 2016.

[23] N. J. Strange, D. Landau, J. Longuski, and P. Chodas, 'Identification of Retrievable Asteroids with the Tisserand Criterion', presented at the AIAA/AAS Astrodynamics Specialist Conference, San Diego, CA, Aug. 2014. doi: 10.2514/6.2014-4458.

[24] A. Bellome, J.-P. Sanchez, J. I. Rico Álvarez, H. Afsa, S. Kemble, and L. Felicetti, 'An Automatic Process for Sample Return Missions Based on Based on Dynamic Programming Optimization', presented at the AIAA SCITECH 2022 Forum,

Copyright ©2022 by Mr. Hadrien AFSA. Published by the IAF, with permission and released to the IAF to publish in all forms.

San Diego, CA & Virtual, Jan. 2022. doi: 10.2514/6.2022-1477.

[25] Y. Chen, H. Baoyin, and J. Li, 'Accessibility of Main-Belt Asteroids via Gravity Assists', *J. Guid. Control Dyn.*, vol. 37, no. 2, pp. 623–632, Mar. 2014, doi: 10.2514/1.58935.

[26] P. Sun, H. Yang, and S. Li, 'Accessibility of near-Earth asteroids and main-belt asteroids in a gravity-assisted multi-target mission', *Planet. Space Sci.*, vol. 182, p. 104851, Mar. 2020, doi: 10.1016/j.pss.2020.104851.

[27] M. Okutsu and J. M. Longuski, 'Mars Free Returns via Gravity Assist from Venus', *J. Spacecr. Rockets*, vol. 39, no. 1, pp. 31–36, Jan. 2002, doi: 10.2514/2.3778.

[28] D. G. Yárnoz, C. H. Yam, S. Campagnola, and Y. Kawakatsu, 'Extended Tisserand-Poincaré graph and multiple lunar swingby design with Sun perturbation'.

[29] M. Pugliatti, 'The Extended Tisserand-Poincaré graph for multi-body trajectory design', Delft University of Technology, 2018. [Online]. Available: https://repository.tudelft.nl/islandora/object/uuid%3A0ab75236-058a-4609-9c22-78ef17b8ede4

[30] N. Ozaki *et al.*, 'Mission Design of DESTINY+: Toward Active Asteroid (3200) Phaethon and Multiple Small Bodies', *Acta Astronaut.*, vol. 196, pp. 42–56, Jul. 2022, doi: 10.1016/j.actaastro.2022.03.029.

[31] S. Campagnola *et al.*, 'Mission Analysis for the EM-1 CubeSats EQUULEUS and OMOTENASHI', *IEEE Aerosp. Electron. Syst. Mag.*, vol. 34, no. 4, pp. 38–44, Apr. 2019, doi: 10.1109/MAES.2019.2916291.

[32] S. Campagnola, P. Skerritt, and R. P. Russell, 'Flybys in the planar, circular, restricted, three-body problem', *Celest. Mech. Dyn. Astron.*, vol. 113, no. 3, pp. 343–368, Jul. 2012, doi: 10.1007/s10569-012-9427-x.

[33] L. Malyshkin, 'The Keplerian Map for the Planar Restricted Three-Body Problem as a Model of Comet Evolution', *Icarus*, vol. 141, no. 2, pp. 341–353, Oct. 1999, doi: 10.1006/icar.1999.6174.

[34] S. Campagnola, B. B. Buffington, and A. E. Petropoulos, 'Jovian tour design for orbiter and lander missions to Europa', *Acta Astronaut.*, vol. 100, pp. 68–81, Jul. 2014, doi: 10.1016/j.actaastro.2014.02.005.

[35] S. Campagnola and Y. Kawakatsu, 'Three-Dimensional Resonant Hopping Strategies and and the Jupiter Magnetospheric Orbiter', *J. Guid. Control Dyn.*, vol. 35, no. 1, pp. 340–344, Jan. 2012, doi: 10.2514/1.53334.

[36] D. de la Torre Sangrà, E. Fantino, R. Flores, O. Calvente Lozano, and C. García Estelrich, 'An automatic tree search algorithm for the Tisserand graph', *Alex. Eng. J.*, vol. 60, no. 1, pp. 1027–1041, Feb. 2021, doi: 10.1016/j.aej.2020.10.028.

[37] A. Bellome, J.-P. Sanchez, L. Felicetti, and S. Kemble, 'Modified tisserand map exploration for preliminary multiple gravity assist trajectory design', presented at the 71st International Astronautical Congress 2020, Oct. 2020. [Online]. Available: https://dspace.lib.cranfield.ac.uk/handle/1826/15914

[38] C. S. Arridge *et al.*, 'Uranus Pathfinder: exploring the origins and evolution of Ice Giant planets', *Exp. Astron.*, vol. 33, no. 2–3, pp. 753–791, Apr. 2012, doi: 10.1007/s10686-011-9251-4.

[39] J. M. Sánchez Pérez, 'Trajectory design of Solar Orbiter'. [Online]. Available: https://www.issfd.org/ISSFD_2012/ISSFD23_IMD1_3.pdf

[40] J. M. Sánchez Pérez and G. I. Varga, 'Solar Orbiter: Consolidated report on mission analysis', Oct. 2018.

[41] G. Lantoine, R. P. Russell, R. L. Anderson, and H. B. Garrett, 'Magnetour: Surfing planetary systems on electromagnetic and multi-body gravity fields', *Acta Astronaut.*, vol. 138, pp. 543–558, Sep. 2017, doi: 10.1016/j.actaastro.2016.12.014.

[42] P. G. Antreasian *et al.*, 'Cassini orbit determination performance during the first eight orbits of the Saturn satellite tour', presented at the AAS/AIAA Astrodynamics Conference, Lake Tahoe, CA, Aug. 2005. [Online]. Available: https://trs.jpl.nasa.gov/bitstream/handle/2014/37673/05-2217.pdf?sequence=1

[43] S. Kemble, *Interplanetary Mission Analysis and Design*. Springer Berlin Heidelberg, 2006. doi: 10.1007/3-540-37645-3.

[44] A. Bellome, J.-P. Sanchez, and S. Kemble, 'Multi-Objective Design of Gravity Assist Trajectories via Graph Transcription and Dynamic Programming', 2022.

[45] ESA, 'JUICE DEFINITION STUDY REPORT (RED BOOK)', 1.0, Sep. 2019. [Online]. Available: https://sci.esa.int/s/wRdzyl8

[46] H. Afsa, 'MSc Thesis: AUTOMATE: Automatic Multi-Gravity Assist Trajectory Design with Tisserand Exploration', Master thesis, Cranfield University, 2021.